Chapter

Metal-Matrix Embedded Phononic Crystals

Suobin Li, Yihua Dou and Linka Niu

Abstract

Metal-matrix embedded phononic crystals (MMEPCs) can be applied for noise and vibration reduction. Metal-matrix embedded phononic crystals (MMEPCs) consisting of double-sided stubs (single "hard" stubs/composite stubs) were introduced. The introduced MMEPCs are deposited on a two-dimensional locally resonant phononic crystal plate that consists of an array of rubber fillers embedded in a steel plate. The lower frequency complete bandgap will be produced in the MMEPCs with composite stubs by decoupling the spring-mass system of the resonator by means of the rubber filler. Then, the out-of-plane bandgap and the in-plane bandgap can be adjusted into the same lowest frequency range by the composite stubs. The broad complete bandgap will be produced in the metal-matrix embedded phononic crystals with single "hard" stubs by producing new kinds of resonance modes (in-plane and out-of-plane analogous-rigid modes) by introducing the single "hard" stubs, and then the out-of-plane bandgap and the in-plane bandgap can be broadened into the same frequency range by the single "hard" stubs. The proposed MMEPCs can be used for noise and vibration reduction.

Keywords: metal-matrix embedded phononic crystals, lower frequency complete bandgap, broad complete bandgap, forming mechanisms of the bandgap, noise, vibration reduction

1. Introduction

In the last two decades, the propagation of elastic waves in periodic composite materials, known as phononic crystals, has attracted increased attention due to their unique physical properties. These properties include phononic bandgaps which define a frequency range where elastic wave propagation is forbidden [1]. The existence of phononic bandgaps enables a variety of potential applications, such as noise and vibration insulation. Two mechanisms cause the formation of bandgaps: Bragg scattering [1] and local resonance [2]. In Bragg scattering, the associated wavelength with the phononic bandgap is of the same order as the periodicity of the structure. This means a huge lattice constant is needed to obtain phononic bandgaps for the low frequency range, which limits applications. To achieve local resonance, the associated wavelength needs to be two orders of magnitude smaller than the Bragg bandgap. A locally resonant bandgap is related to the resonance frequency associated with scattering units and depends less on the periodicity and symmetry of the structure. Therefore, it overcomes the limitation of Bragg bandgaps and permits bandgaps suitable for low frequencies.

The existence of low-frequency locally resonant bandgaps (LRBGs) gives rise to the application of locally resonant phononic crystals (LRPCs) in the reduction of low-frequency vibration and noise [3]. However, it has been a challenging task due to the long wavelength and weak attenuation of the low-frequency waves. In the past years, many LRPCs were proposed to obtain bandgaps in low frequency range or broaden bandgaps in the low frequency range [4–19]. More recently, the propagation of Lamb waves (elastic waves) in phononic crystal plates, which is based on a local resonance mechanism, has attracted attention due to their potential applications in filters, resonators, waveguides, and for vibration insulation. In general, phononic-crystal plates can be classified into two types according to their structural features: flat plates and stubbed plates. The flat phononic-crystal plate consists of a periodical array of holes or periodic inclusions of foreign material in a homogeneous plate [5]. Many previous studies focused on this type of phononic-crystal plates to investigate the bandgap properties. It is not easy to obtain lower frequency phononic bandgaps using a flat phononic-crystal plate. Stubbed phononic-crystal plates can be classified into two types: the single-sided stubbed phononic-crystal plate and the double-sided stubbed phononic-crystal plate. The single-sided stubbed phononic-crystal plate [3] consists of a square array of stubs on one side of a homogeneous plate [6]. Subsequently, many researchers investigated the effects of material properties and geometric parameters on the BG of the single-sided stubbed phononic-crystal plate and found that the mass and the geometric parameter effect can help tune the bandgap into low frequencies [8]. Later, a novel single-sided stubbed phononic-crystal plate was proposed. It consists of a square array of stubs on one side of a two-dimensional binary locally resonant phononic plate. It can increase of the relative bandwidth over the classical single-sided stubbed plate [12]. The double-sided stubbed phononic-crystal plate consists of a square array of stubs on both sides of a homogeneous plate. It can reduce the bandgap compared to a single-sided stubbed phononic-crystal plate [9]. Recently, a novel double-sided stubbed phononic-crystal plate was proposed. Unlike the classical double-sided stubbed phononic-crystal plate, it can shift the bandgap into the lower frequency range [13].

However, because there are three different modes for a plate, and they can only be coupled separately to special resonating modes of the resonators, the gaps for in-plane and out-of-plane plate modes can hardly be overlapped with each other in lower frequencies due to the coupling of the spring-mass system of the resonator, and thus the lower complete bandgaps (below 100 Hz) are difficult to obtain. As a result, the BGs of these disused PC plates are usually located in the frequency range above 300 Hz. However, the frequency of most of the ambient vibration in practical cases is distributed over a wide frequency range from 20 to 250 Hz. Also, the broad bandgaps for in-plane and out-of-plane plate modes can hardly be overlapped with each other in same frequency range due to the weak coupling between the resonator mode and the plate mode, and thus the broad complete bandgaps are difficult to obtain too. At the same time, a common feature of phononic-crystal plates is matrix structures made of nonmetallic materials. However, most mechanical structures typically consist of metals, and a phononic-crystal plate with a nonmetallic material matrix can hardly be used for vibration and noise reduction in mechanical engineering. Recently, a metal-matrix embedded phononic crystal which consists of periodic double-sided stepped resonators deposited on a two-dimensional phononic plate within a steel matrix was proposed. It is found that the bandwidth is increased, but the opening location of the bandgap is higher (1000 Hz) [19]. In other words, the extension of the bandwidth into the lower frequency range remains a challenging task for a metal-matrix embedded phononic crystal.

Thus, how to adjust the in-plane and out-of-plane gaps overlapping with each other in the lower frequencies (below 100 Hz) or increasing the in-plane and out-of-plane gaps in the same range is an important issue for the control of the vibration in a practical case.

In this chapter, two kinds of metal-matrix embedded phononic crystals are introduced. The one is called the lower frequency complete bandgap metal-matrix embedded phononic crystals [14] because it can produce lower frequency complete bandgap, and the other is called the broad complete bandgap metal-matrix embedded phononic crystals [20] because it can produce broad complete bandgap.

2. The method of calculation

In order to investigate the band properties of the metal-matrix embedded phononic crystals, a series of calculations on dispersion relations and transmission spectra are conducted with FEM based on the Bloch theorem. For the calculation of the dispersion relations, the governing field equations for elastic wave propagation in solids are given by

$$\sum_{j=1}^{3}\frac{\partial}{\partial x_j}\left(\sum_{l=1}^{3}\sum_{k=1}^{3}c_{ijkl}\frac{\partial u_k}{\partial x_l}\right)=\rho\frac{\partial^2 u_i}{\partial t^2}\ (i=1,2,3) \tag{1}$$

where ρ is the mass density, t is the time, u_i is the displacement, c_{ijkl} are the elastic constants, and x_j (j = 1, 2, 3) represents the coordinate variables x, y, and z, respectively. According to the Bloch theorem, in the FEM formulation, the displacement field can be expressed as

$$u(r)=e^{i(k\cdot r)}u_k(r) \tag{2}$$

where u is the displacement at the nodes and r is the position vector located at the boundary nodes. The Bloch wave vector $k = (k_x, k_y)$ is the wave vector limited to the first Brillouin zone of the reciprocal lattice. Since the metal-matrix embedded phononic crystal plate is periodic in the xy-direction and finite in the z-direction, only the unit cell (shown as in **Figure 1(b)** or **Figure 3(b)**) needs to be considered in the FEM calculation when the Bloch theorem is adopted on the boundaries between the unit cell and its two adjacent cells, given by

$$u_i(x+a,y+a)=e^{i(k_x\cdot a+k_y\cdot a)}u_i(x,y)(i=x,y,z) \tag{3}$$

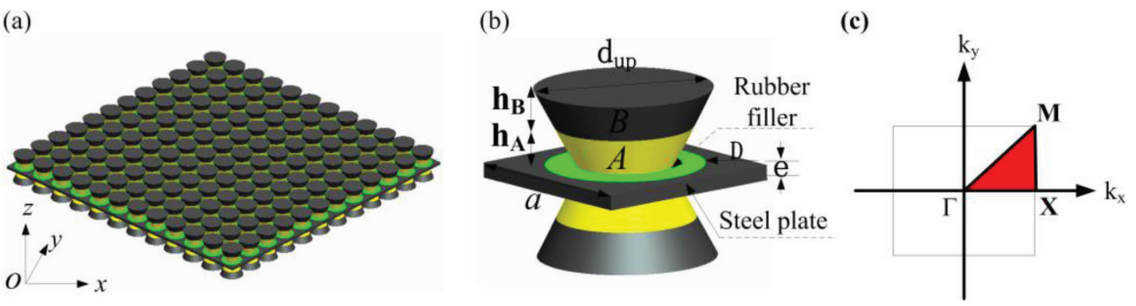

Figure 1.
(a and b) Schematic of the part and the unit cell of the lower frequency complete bandgap metal-matrix embedded phononic crystals, respectively. (c) The corresponding first irreducible Brillouin zone (red region) and the high-symmetry M, Γ, and X.

where the elastic displacement vector is denoted by u; the position vectors are denoted by x, y, and z; and k_x and k_y are the Bloch wave vectors limited in the irreducible first Brillouin zone (shown as in **Figure 1(c)** or **Figure 3(c)**). The Bloch calculation gives the eigenfrequencies and the corresponding eigenvectors, and then the dispersion relationships can be obtained by changing the wave vector in the first irreducible Brillouin zone.

To further demonstrate the existence of the bandgaps of the metal-matrix embedded phononic crystals, the transmission spectra for a structure with finite units along the x- or y-direction is calculated by using FEM. The acceleration excitation source is incident from one side (left side) of the finite structure and propagates along the x- or y-direction. The corresponding transmitted acceleration is recorded on another side (right side) of the structure. The transmission spectrum is defined as

$$TL = 10 \log\left(\frac{\alpha_o}{\alpha_i}\right) \tag{4}$$

where α_o and α_i are the output and input accelerations of the metal-matrix embedded phononic crystals, respectively. Finally, the transmission spectra can be obtained by changing the excitation frequency of the incident acceleration.

3. The model and the results

3.1 The lower frequency complete BG phononic crystals

3.1.1 The model of the phononic crystals

The lower frequency bandgap metal-matrix embedded phononic crystal [14] was composed of a square array of composite taper stubs on both sides of a two-dimensional binary locally resonant PC plate which composes an array of rubber fillers embedded in the steel plate. **Figure 1(a)** and **(b)** shows part of the proposed structure and its unit cell, respectively.

In the lower frequency bandgap metal-matrix embedded phononic crystals, the taper stub is composed of the A taper cap and the B which is located on the taper A. The geometrical parameters of the structure are defined as follows: the diameter of the rubber filler, the steel plate thickness, and the lattice constant are denoted by D, e, and a, respectively; the height and the diameter of the taper stub are denoted by h (h_A for taper A and h_B for taper B) and d (the upper diameter of taper stub is denoted by d_{up}, and the lower diameter is denoted by d_{low}), respectively. The material parameters used in the calculations are listed in **Table 1**. The taper A and the taper B are rubber and steel, respectively.

3.1.2 The results of the phononic crystals

Through the use of the finite element method, the systems described in **Figure 1** were studied numerically. The band structures and displacement vector

Material	Mass density (kg/m^3)	Young's modulus (10^{6}N/m^2)	Poisson's ratio
Steel	7800	210,000	0.29
Rubber	1300	0.1175	0.47

Table 1.
Material parameters in calculations.

fields were computed according to the Bloch theorem. The single-unit cell (as shown in **Figure 3(b)**) is determined by the periodicity of the structure. The following structure parameters are used: D = 8 mm, e = 1 mm, a = 10 mm, h = 5 mm (h_A = h_B = 2.5 mm), d_{up} = 9 mm, and d_{low} = 5 mm, respectively.

It can be observed that there are 13 bands within 0–200 Hz in **Figure 2(a)**. Besides the traditional plate modes, which are the in-plane modes (mainly the symmetric Lamb modes, such as modes S_2) and the out-of-plane modes (mainly the antisymmetric Lamb modes, such as mode A_2), lots of flat modes (such as modes S_1, A_1, F_2), which are the resonant modes of the composite taper stubs, can be found. The bandgaps (one in-plane bandgap, one out-of-plane bandgap, and one complete bandgap), as a result of the coupling of the two kinds of modes mentioned above, appear. The in-plane bandgap (blue-dashed area: the frequency bands in which no in-plane modes) is due to the coupling between the in-plane modes (modes S_2) and the corresponding flat modes (modes S_1). It ranges from 53 to 93 Hz (between the fifth and eighth bands). The absolute bandwidth of it is 40 Hz. The out-of-plane bandgap (green-dashed area: the frequency bands in which no out-of-plane modes) is due to the coupling between the out-of-plane modes (mode A_2) and the corresponding flat modes (mode A_1). It ranges from 59 to 154 Hz (between the sixth and ninth bands), and the absolute bandwidth is 95 Hz; the complete bandgap (red-dashed area: the frequency bands in which neither in-plane modes nor out-of-plane modes) is due to the overlap between the in-plane bandgap and the out-of-plane bandgap. It ranges from 59 to 93 Hz (between the sixth and eighth bands). The absolute bandwidth of it is 34 Hz. It can be observed that the location of the bandgap shifts into lower frequency (below 100 Hz), but the bandwidth is very narrow.

As a comparison, we also calculated the band structures of the transition PC plate composed of double-sided composite taper stubs deposited on a homogeneous steel plate and the classical PC plate which was proposed by Assouar [9]. They are shown in **Figure 2(b)** and **(c)**, respectively. Their complete bandgaps (red-dashed areas) are both due to the overlap between the second in-plane bandgap and the first out-of-plane bandgap. It can be found clearly that the introduction of the

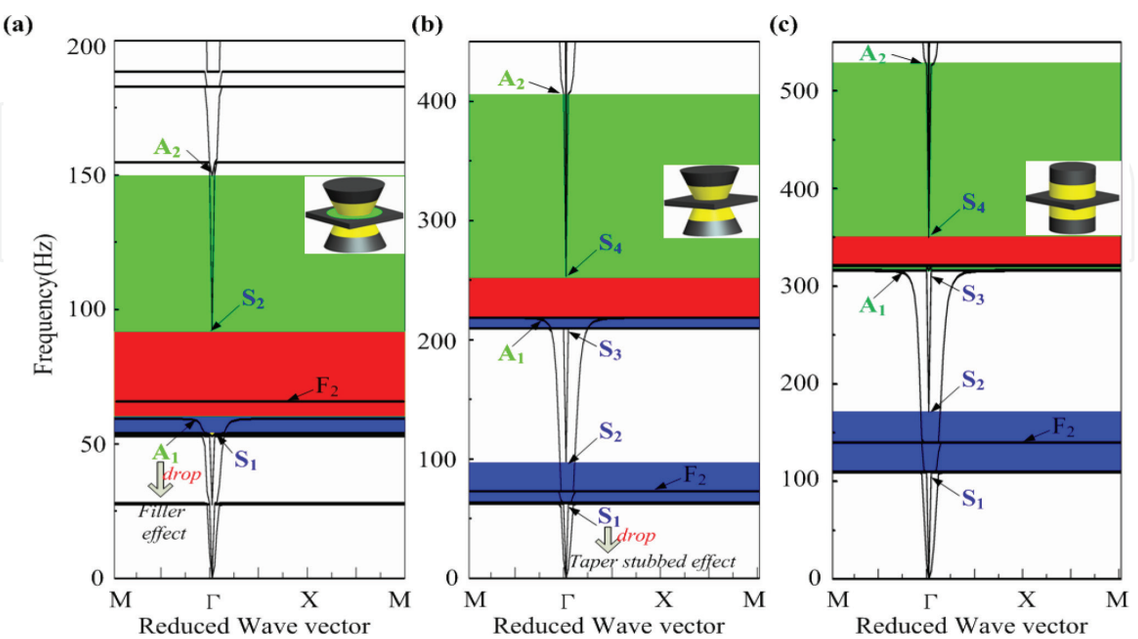

Figure 2.
Band structures of (a) the lower frequency complete bandgap metal-matrix embedded PC plate, (b) the transition PC plate, and (c) the classical PC plate. The insets are the schematic view of the unit cell of the corresponding structure. The red, blue, and yellow shadow regions denote the complete, in-plane, and out-of-plane bandgaps, respectively.

proposed structure gives rise to a significant lowering of the opening location of the first complete bandgap by a factor of 5.5 compared with the classical PC plate. Compared with the classical PC plate, introducing the double-sided composite taper stubs, the locations of both the in-plane and out-of-plane bandgaps are lowered, but the out-of-plane bandgap is always overlapped with the second in-plane bandgap; when introducing the rubber filler, the location of the in-plane bandgap is kept stationary, and the out-of-plane bandgap is shifted to lower frequency (59 Hz) overlapped with the first in-plane bandgap. Finally, a complete bandgap is generated in lower frequency (below 100 Hz). Therefore, the double-sided taper stub has a direct effect on the lowering of the location of the in-plane bandgaps (53 Hz), and the rubber filler has a direct effect on the lowering of the location of the out-of-plane bandgaps (59 Hz). It makes the out-of-plane bandgaps overlap with the first in-plane bandgap and leads to a complete bandgap in lower frequencies [14].

3.2 The broad complete BG phononic crystals

3.2.1 The model of the phononic crystals

The broad complete bandgap metal-matrix embedded phononic crystal [18] was composed of a square array of single "hard" cylinder stubs on both sides of a two-dimensional binary locally resonant PC plate which composes of an array of rubber fillers embedded in the steel plate. **Figure 3(a)** and **(b)** shows part of the structure and its unit cell, respectively.

The metal-matrix embedded phononic crystals with single "hard" cylinder stubs which consist of "hard" stub such as steel stubs contact with rubber filler. The geometrical parameters of the structure are defined as follows: the diameter of the rubber filler, the steel plate thickness, and the lattice constant are denoted by D, e, and a, respectively; the height and the diameter of the stub are denoted by h and d, respectively. The material parameters used in the calculations are listed in **Table 1**.

3.2.2 The results of the phononic crystals

Through the use of the finite element method, the systems described in **Figure 3** were studied numerically. The band structures and displacement vector fields were computed according to the Bloch theorem. The single-unit cell (as shown in **Figure 3(b)**) is determined by the periodicity of the structure. The following structure parameters are used: D = 8 mm, e = 1 mm, a = 10 mm, h = 2.5 mm, and d = 7.5 mm.

There are 12 bands within 0–600 Hz (see **Figure 4(a)**). Besides the traditional plate modes, which are the in-plane modes (such as mode S_2) and the out-of-plane modes (such as mode A_2), many flat modes (such as modes S_1, A_1, F_1), which are

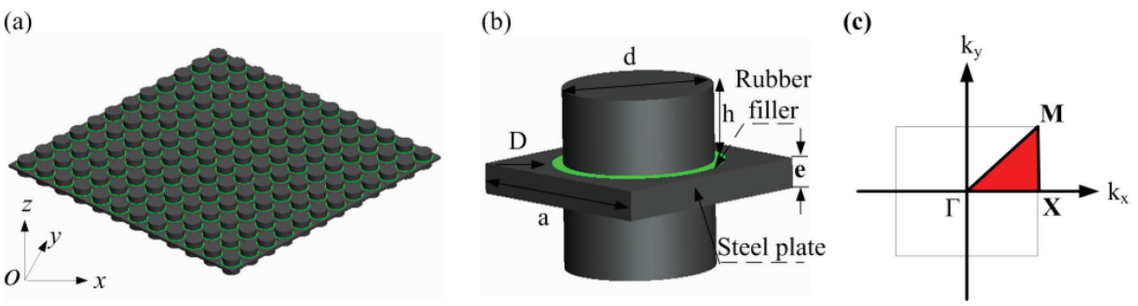

Figure 3.
(a and b) Schematic of the part and the unit cell of the broad complete bandgap metal-matrix embedded phononic crystals, respectively. (c) The corresponding first irreducible Brillouin zone (red region) and the high-symmetry M, Γ, and X.

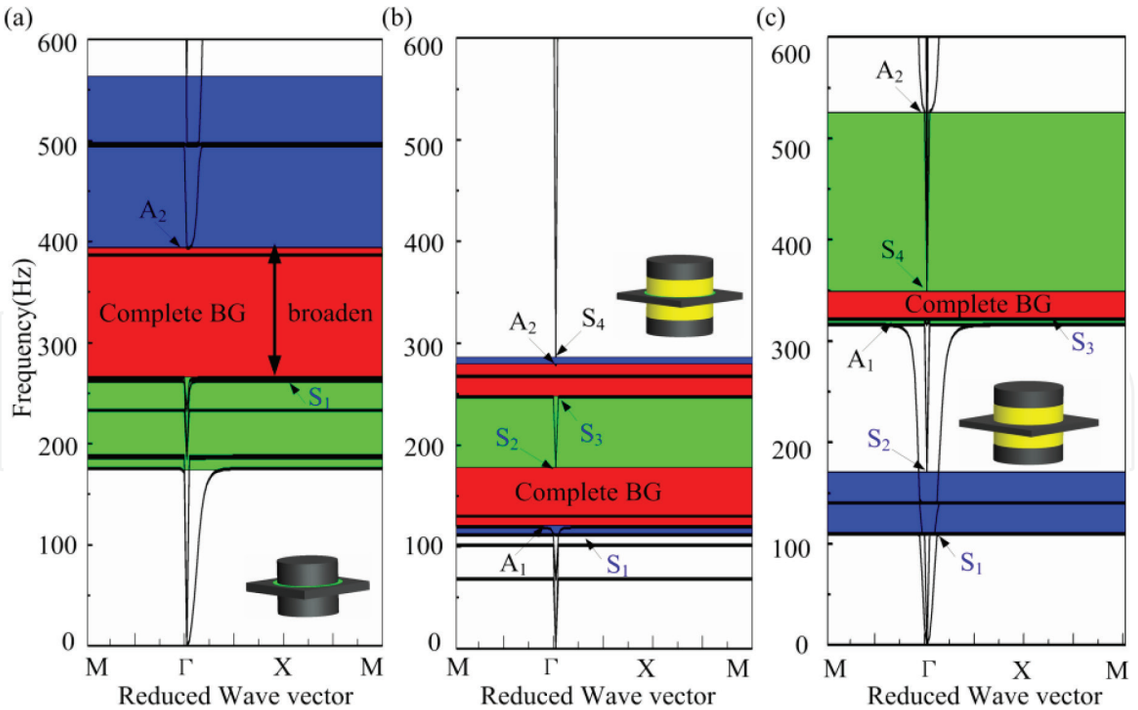

Figure 4.
Band structures of (a) the broad complete bandgap metal-matrix embedded phononic crystals, (b) the transition PC plate, and (c) the classical PC plate. The insets are the schematic view of the unit cell of the corresponding structure. The red, blue, and yellow shadow regions denote the complete, in-plane, and out-of-plane bandgaps, respectively.

the resonant modes of the single "hard" cylinder stubs, can be found. The bandgaps (one in-plane bandgap, one out-of-plane bandgap, and one complete bandgap) appear due to coupling between the two modes. The in-plane bandgap (**Figure 4(a)**: blue-dashed area) is due to coupling between the in-plane modes S_2 and the corresponding flat mode S_1. It ranges from 260 to 573 Hz (between the sixth and twelfth bands). The absolute bandwidth is 313 Hz. The out-of-plane bandgap (**Figure 4(a)**: green-dashed area) is due to coupling between the out-of-plane mode A_2 and the corresponding flat modes A_1. It ranges from 187 to 396 Hz (between the third and eighth bands), and the absolute bandwidth is 209 Hz; the complete bandgap (**Figure 4(a)**: red-dashed area) is due to the overlap between the in-plane bandgap and the out-of-plane bandgap. It ranges from 260 to 396 Hz (between the sixth and eighth bands). The absolute bandwidth is 136 Hz.

As a comparison, we also calculated the band structures of the transition PC plate composed of double-sided composite cylinder stubs deposited on a two-dimensional locally resonant phononic crystal plate that consists of an array of rubber fillers embedded in a steel plate and the classical PC plate which was proposed by Assouar [9]. They are shown in **Figure 4(b)** and **(c)**, respectively. For the classical phononic-crystal plate, its first complete bandgap (red-dashed area) is caused by the overlap between the second in-plane bandgap and the first out-of-plane bandgap. The associated absolute bandwidth is 29 Hz. For the transition phononic-crystal plate, the bandgaps are lowered after introducing the rubber filler, such that both the out-of-plane bandgap and in-plane bandgap were lowered. However, the out-of-plane bandgap is lowered more and overlaps with two in-plane bandgaps (the first and the second in-plane bandgaps). This causes the complete bandgaps to be increased, but the absolute bandwidth is also narrow (78 Hz). These phenomena confirm that the single "hard" cylinder stub has a special effect on the bandwidth and the bandwidth can be increased by introducing it. This occurs mainly because the in-plane bandgap is increased by introducing the single "hard"

cylinder stub in the broad complete bandgap metal-matrix embedded phononic crystals. The absolute bandwidth of the in-plane bandgap is increased by a factor of 3.37 compared with a classical phononic-crystal plate [18].

4. Forming mechanisms of the BGs of the phononic crystals

4.1 Forming mechanisms of the lower frequency complete BGs

In order to study the physical mechanism for the occurrence of the lower frequency complete bandgap in the metal-matrix embedded phononic crystals [14, 18], several specific resonance modes (mode A_1, mode S_1), which correspond to the lower edge of the first bandgap (out-of-plane and in-plane bandgap), and several specific traditional plate modes (mode A_2, mode S_2), which correspond to the upper edge of the first bandgap (in-plane and out-of-plane bandgaps), are extracted.

4.1.1 Forming mechanisms of the lower out-of-plane BGs

Figure 5 displays the magnitude of the total displacement vector of a unit cell of the lower frequency complete bandgap metal-matrix embedded phononic crystals (**Figure 2(a)**), the transition structure (**Figure 2(b)**), and the classical structure (**Figure 2(c)**), respectively. They correspond to the upper and lower edge of the out-of-plane bandgap of each structure. The mode A_2 is an antisymmetric Lamb mode of the plate. The steel plate vibrates along the z-axis, while the stub remains stationary. In the frequencies, the antisymmetric Lamb mode will be activated, and the out-of-plane waves propagate through the PC plate in the antisymmetric Lamb mode. When the frequency of the out-of-plane waves is near the first nature frequency of the stub resonator, the resonant mode A_1 will be activated. The stub vibrates along the z-direction, and it gives a reacting force to the plate against the plate that vibrates along the z-direction. In that case, the out-of-plane waves are not capable of propagating through the PC plate. As a result, an out-of-plane bandgap is opened. Within the out-of-plane bandgap, the reacting force is still applied on the

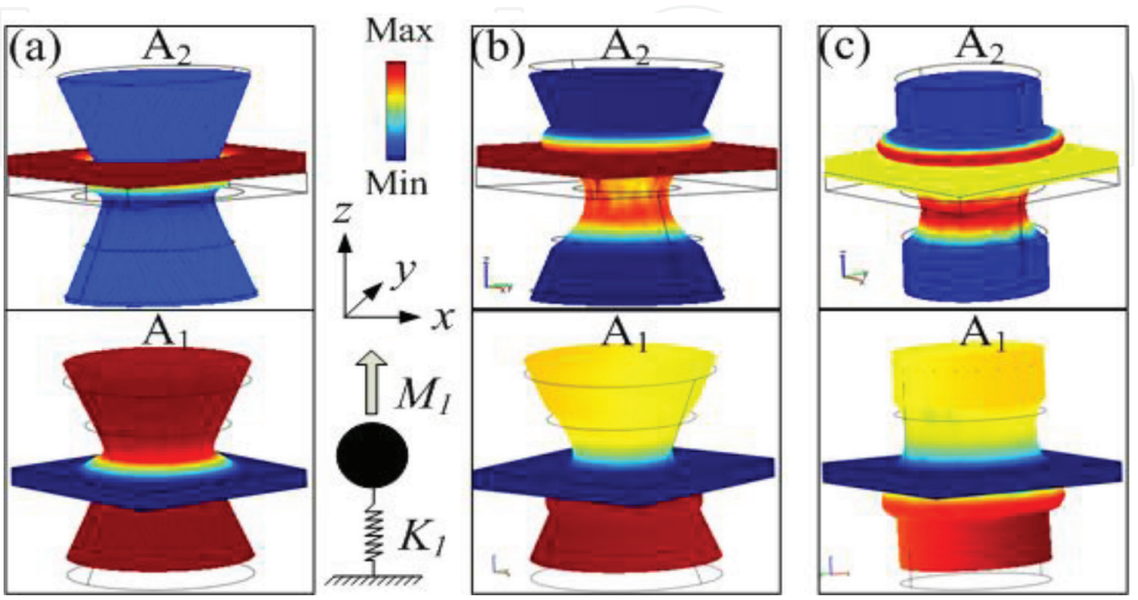

Figure 5.
The total displacement vector fields of the modes (resonant mode A_1 and antisymmetric Lamb mode A_2) (a) correspond to **Figure 2(a)**, *(b) correspond to* **Figure 2(b)**, *and (c) correspond to* **Figure 2(c)**.

plate and prevents the propagation of the out-of-plane waves. The frequency of the out-of-plane waves deviates from the nature frequency of the mode A_1, according to the modal superposition principle which can be described as

$$z = \eta_1 A_1 + \eta_2 A_2 + \cdots + \eta_n A_n \tag{5}$$

where z denotes the response of the plate and η_n denotes the modal participation factor of the mode A_n. The modal participation factor η_1 of the mode A_1 becomes small, leads the reacting force to becoming weak, and then disappears, and the antisymmetric Lamb mode A_2 is released again. As a result, the out-of-plane bandgap is closed. The formation mechanism of the bandgaps is shown in **Figure 6**. As the frequency of the out-of-plane waves deviates from the nature frequency of the resonator mode, the modal participation factors of it become small, lead the reacting force to becoming weak, and then disappear; the out-of-plane bandgap is closed. It can be concluded that the out-of-plane bandgap of the system is formed due to the coupling between the flat mode A_1 and the antisymmetric Lamb mode A_2 which is established based on the modal superposition principle.

The opening location of the out-of-plane bandgap is determined by the nature frequency of the resonant mode A_1. The vibration process of the resonant mode A_1 can be understood as a mass-spring system whose frequency is determined by the formula

$$f_1 = \frac{1}{2\pi}\sqrt{\frac{K_1}{M_1}} \tag{6}$$

where K_1 is the spring stiffness and M_1 is the lump mass. For the classical structure, the rubber stub (denoted by A) acts as a spring, and the cap steel stub (denoted by B) acts as a mass ($M_1 = M_B$, where M_B denotes the mass of stub B). For the lower frequency complete bandgap metal-matrix embedded phononic crystals, it can be found that the displacement fields are distributed in the whole stub and manifest an "analogous-rigid mode" of the whole stub, since the whole stub bodily moves along the z-axis with weak constrain, and the natural frequency is not zero. In this case, the rubber filler acts as a spring, and the whole stub acts as a mass; thus, the frequency is shifted to a lowest frequency range. It can be concluded that the out-of-plane bandgap is adjusted into lower frequency range by the rubber filler.

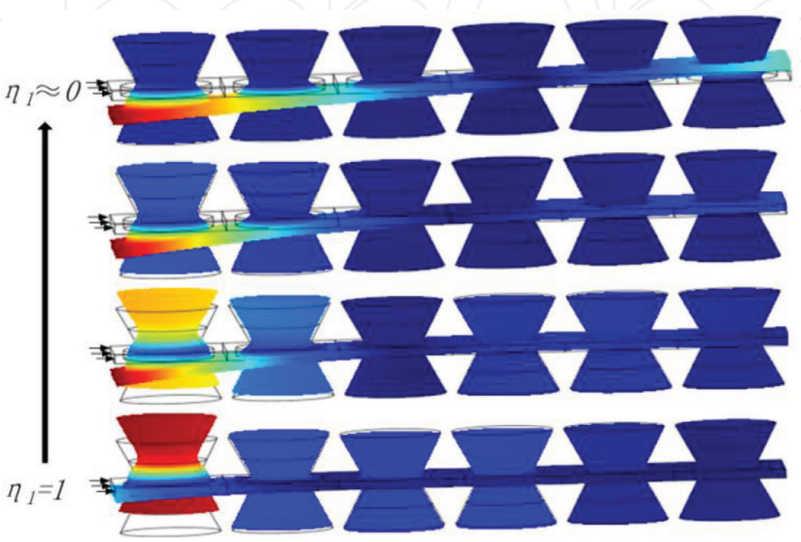

Figure 6.
The formation mechanism of the out-of-plane bandgaps of the lower frequency complete bandgap metal-matrix embedded phononic crystals.

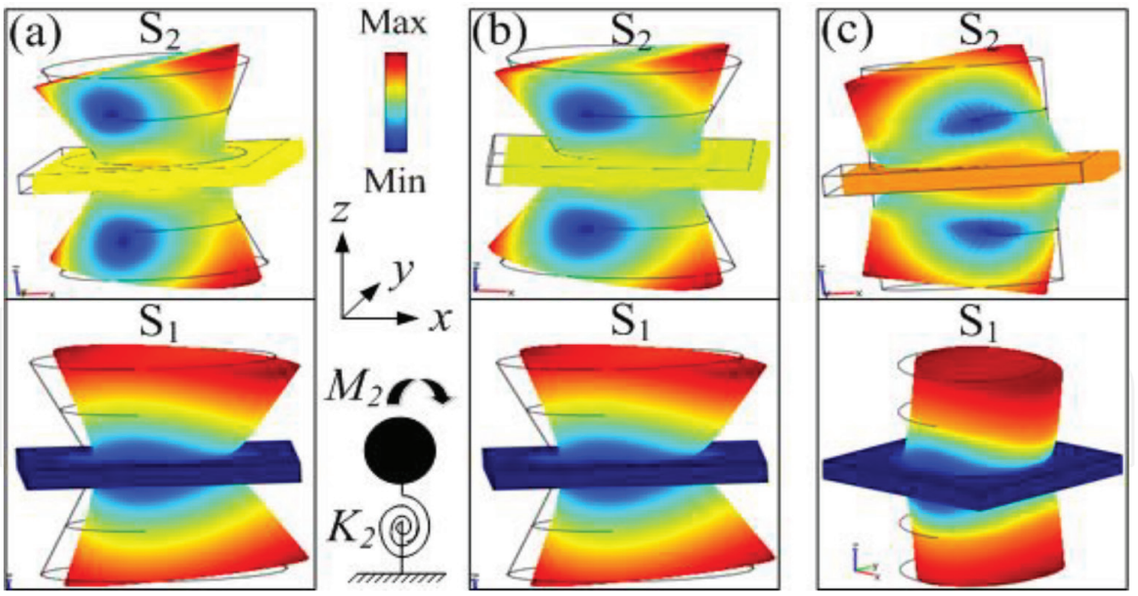

Figure 7.
The total displacement vector fields of the modes (resonant mode S_1, symmetric Lamb mode S_2) (a) correspond to ***Figure 2(a)****, (b) correspond to* ***Figure 2(b)****, and (c) correspond to* ***Figure 2(c)****.*

4.1.2 Forming mechanisms of the lower in-plane BGs

Figure 7 displays the magnitudes of the total displacement vectors of a unit cell of the lower frequency complete bandgap metal-matrix embedded phononic crystals (**Figure 7(a)**), the transition structure (**Figure 7(b)**), and the classical structure (**Figure 7(c)**), respectively. They correspond to the upper and lower edges of the first in-plane bandgap of each structure. The mode S_2 is a symmetric Lamb mode of the plate. The steel plate vibrates along the *xy*-plane, while the stubs "swing" in the opposite direction. In the frequencies, the symmetric Lamb mode S_2 will be activated, and the in-plane waves propagate through the PC plate in the symmetric Lamb mode. When the frequency of the in-plane waves is near the first nature frequency of stub resonator, the resonant mode S_1 (flat mode) will be activated. The stub "swings" along a plane which is vertical to the *xy*-plane, and it gives a reacting force to the plate to prevent the plate to vibrate along the *xy*-plane. In that case, the in-plane waves are not capable of propagating through the PC plate. As a result, an in-plane bandgap is opened. Within the in-plane bandgap, the reacting force is still applied on the plate and prevents in-plane waves that propagate. The frequency of the in-plane waves deviates from the nature frequency of the resonant mode S_1, according to the modal superposition principle. Which can be described as

$$xy = \eta_1 S_1 + \eta_2 S_2 + \cdots + \eta_n S_n \tag{7}$$

where *xy* denotes the response of the plate and η_n denotes the modal participation factor of the mode S_n. The modal participation factor η_1 of the mode S_1 becomes small, leads the reacting force to becoming weak, and then disappears, and then the symmetric Lamb mode S_2 is released again. As a result, an in-plane bandgap is closed. It can be concluded that the first in-plane bandgap of the system is formed due to the coupling between the flat mode S_1 and the symmetric Lamb mode S_2 which is established according to the modal superposition principle. The opening location is determined by the nature frequency of the resonant mode S_1. The resonant mode S_1 can also be understood as a "mass-spring" system whose frequency is determined by the formula

$$f_2 = \frac{1}{2\pi}\sqrt{\frac{K_2}{M_2}} \tag{8}$$

where K_2 is the tensional stiffness of the spring and M_2 is the lump mass. For the three PC plates, the rubber stub A mainly acts as a spring, and the cap steel stub B acts as a mass ($M_2 = M_B$). As the stiffness of the taper rubber stub is weaker than that of the cylinder stub, the location of the in-plane bandgap is adjusted into lower frequency range.

4.1.3 Forming mechanisms of the lower complete BGs

We can conclude from the above investigations that the resonator in the metal-matrix embedded phononic crystals can be considered as a spring-mass system, as shown in **Figures 6** and 7. The spring-mass system includes two subsystems. The first one is the K_1-M_1 subsystem (also refer to **Figure 6**). Its local resonance mode is coupled with the antisymmetric Lamb mode of the plate according to the modal superposition principle, and then the out-of-plane bandgap is generated. The other one is the K_2-M_2 subsystem (also **Figure** 7). Its local resonance mode is coupled with the symmetric Lamb mode of the plate according to the modal superposition principle and is responsible for the formation of the in-plane bandgaps. The opening locations of the in-plane and out-of-plane BGs depend on the natural frequencies of the two subsystems.

As for the classical and the transition metal-matrix embedded phononic crystals, the steel stub (stub B) acts as a mass, and the rubber stub (stub A) acts as a spring, which leads to the coupling between the K_1-M_1 subsystem and K_2-M_2 subsystem. Therefore, it is difficult to adjust the in-plane and out-of-plane bandgaps separately. In the lower frequency bandgap metal-matrix embedded phononic crystals, the rubber filler acts as the stiffness K_1, the stub A acts as the stiffness K_2, the whole stub acts as the mass M_1, and the stub B acts as the mass M_2. As a result, the coupling between the K_1-M_1 subsystem and the K_2-M_2 subsystem can be decoupled. Moreover, the mass M_1 is magnified due to the "analogous-rigid mode" of the whole stub. Therefore, the out-of-plane bandgap can be adjusted into the lowest frequency range. Additionally, the stiffness K_2 can be reduced by introducing the taper stub, and thus the in-plane bandgaps can be adjusted into the lowest frequency range. As a result, the two bandgaps can be overlapped with each other in the lowest frequency, and finally a lowest complete bandgap is formed [14].

4.2 Forming mechanisms of the broad complete BGs

In order to study the physical mechanism for the occurrence of a broad complete bandgap in the metal-matrix embedded phononic crystals, several specific resonance modes (modes A_1 and S_1), which correspond to the lower edge of the first bandgap (out-of-plane and in-plane bandgap), and several specific traditional plate modes (mode A_2 and S_2), which correspond to the upper edge of the first bandgap (in-plane and out-of-plane bandgaps), are extracted.

4.2.1 Forming mechanisms of the broad out-of-plane BGs

Figure 8 displays the magnitude of the total displacement vector of a unit cell of the broad complete bandgap metal-matrix embedded phononic crystals (**Figure 8(a)**), the transition PC plate (**Figure 8(b)**), and the classical PC plate (**Figure 8(c)**), respectively. They correspond to the upper and lower edge of the out-of-plane bandgap of each structure. The mode A_2 is an antisymmetric Lamb mode of the plate. The steel plate vibrates along the z-axis, while the stub remains

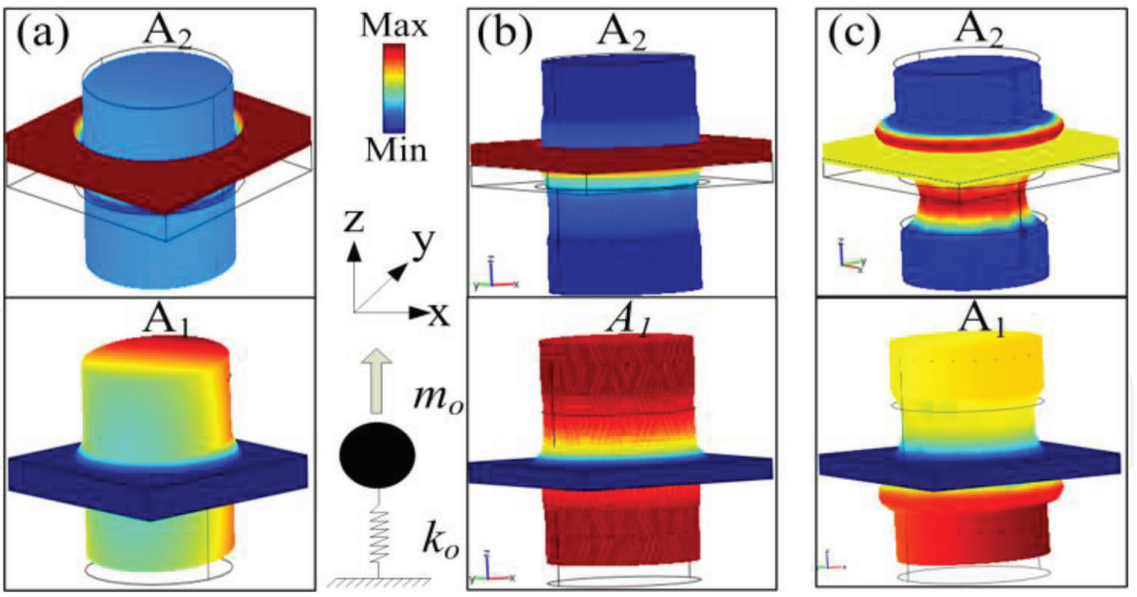

Figure 8.
The total displacement vector fields of the modes (resonant mode A1 and antisymmetric Lamb mode A2) (a) correspond to ***Figure 4(b)****, (b) correspond to* ***Figure 4(b)****, and (c) correspond to* ***Figure 4(c)****.*

stationary. With regard to the frequencies, the antisymmetric Lamb mode will be activated, and the out-of-plane waves propagate through the phononic-crystal plate in the antisymmetric Lamb mode. When the frequency of the out-of-plane waves is near the first nature frequency of the stub resonator, the resonant mode A_1 will be activated. The stub vibrates along the z-direction and produces a reacting force for the plate, and the plate vibrates along the z-direction. In this case, the out-of-plane waves are not capable of propagating through the phononic-crystal plate. As a result, an out-of-plane bandgap is created. The bandwidth is determined by the coupling between the resonance mode A_1 and the traditional plate A_2 mode.

The coupling strength between the resonance mode A_1 and the traditional plate A_2 mode is determined by the formula

$$F = k_o s_T \tag{9}$$

where s_T is the vibration amplitude of the stub and k_o is the spring stiffness.

For the classical structure, the formation mechanism of the out-of-plane bandgap is shown in **Figure 9(b)**. The hard stub (rigid body) vibrates along the z-direction and generates a reacting force through the soft stub (flexible body) to the plate against the plate vibrating along the z-direction. The soft stub acts as a spring, while the hard stub acts as a mass ($k_o = k_{sc}$, $m_o = m_h$, where m_h denotes the mass of the hard stub and k_{sc} denotes the compression stiffness of the soft stub) (see **Figure 10(b)**).

For both the broad complete bandgap metal-matrix embedded phononic crystals and the transition PC plate, it can be found that the displacement fields are distributed in the whole stub (see **Figure 8(a)** and **(b)**), respectively. This results in an "out-of-plane analogous-rigid mode" because the whole stub vibrates along the z-axis (out-of-plane) with a weak constraint, while the frequency is non-zero. The displacement fields of its eigenmodes are distributed throughout the whole stub. This means that the whole stub body moves along the z-direction like a rigid body moves in rigid mode. However, the natural frequency is not 0, and the whole stub is constrained by the rubber filler. Therefore, we refer to the concept "rigid mode" and call these types of vibration modes for the whole stub the "out-of-plane analogous-rigid mode." The formation mechanisms for the out-of-plane bandgap of the two structures are shown in **Figure 9(a)** and **(c)**, respectively.

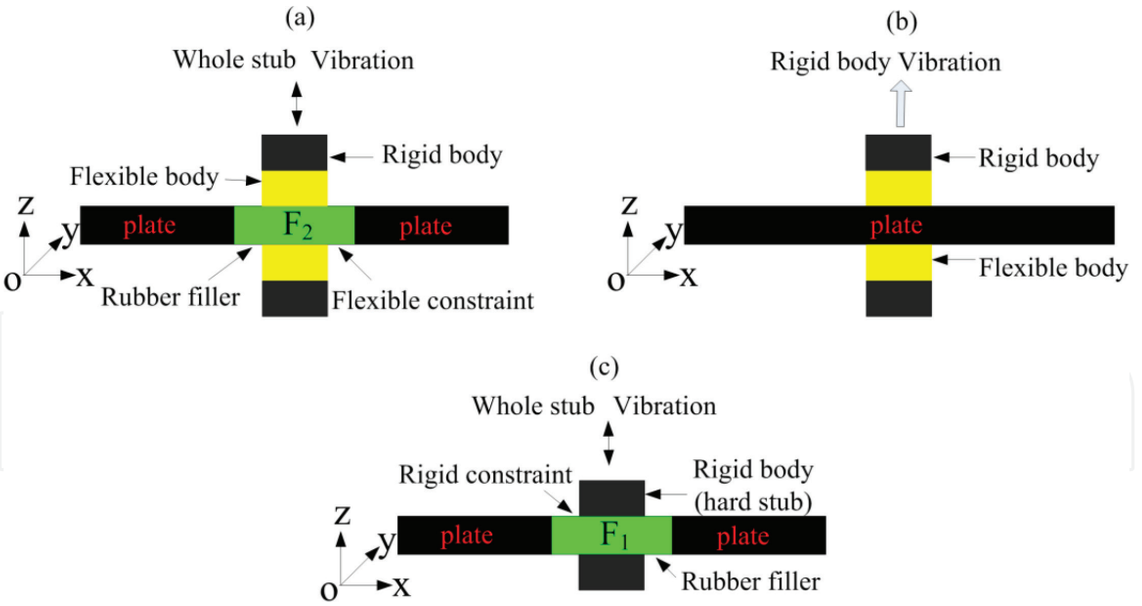

Figure 9.
Formation mechanism of the bandgap for the out-of-plane bandgap of (a) the transition PC plate, (b) the classical PC plate, and (c) the broad complete bandgap metal-matrix embedded phononic crystals.

The whole stub vibrates in the z-direction (out-of-plane) and generates a reacting force. F_1 and F_2 respond to the broad complete bandgap metal-matrix embedded phononic crystals and the transition PC plate, respectively. $F_1 = k_0.s_1 = k_{RT}.s_1$, where k_{RT} is the transverse stiffness of the rubber filler and s_1 is the vibration amplitude of the whole single "hard" stub; $F_2 = k_0.s_2 = k_{RT}.s_2$, where s_2 is the vibration amplitude of the whole composite stub through rubber filler to the plate against the plate vibrates along the z-direction (see **Figure 9(a)** and **(c)**).

In this case, the rubber filler acts as a spring, and the whole stub acts as a mass. The broad complete bandgap metal-matrix embedded phononic crystals

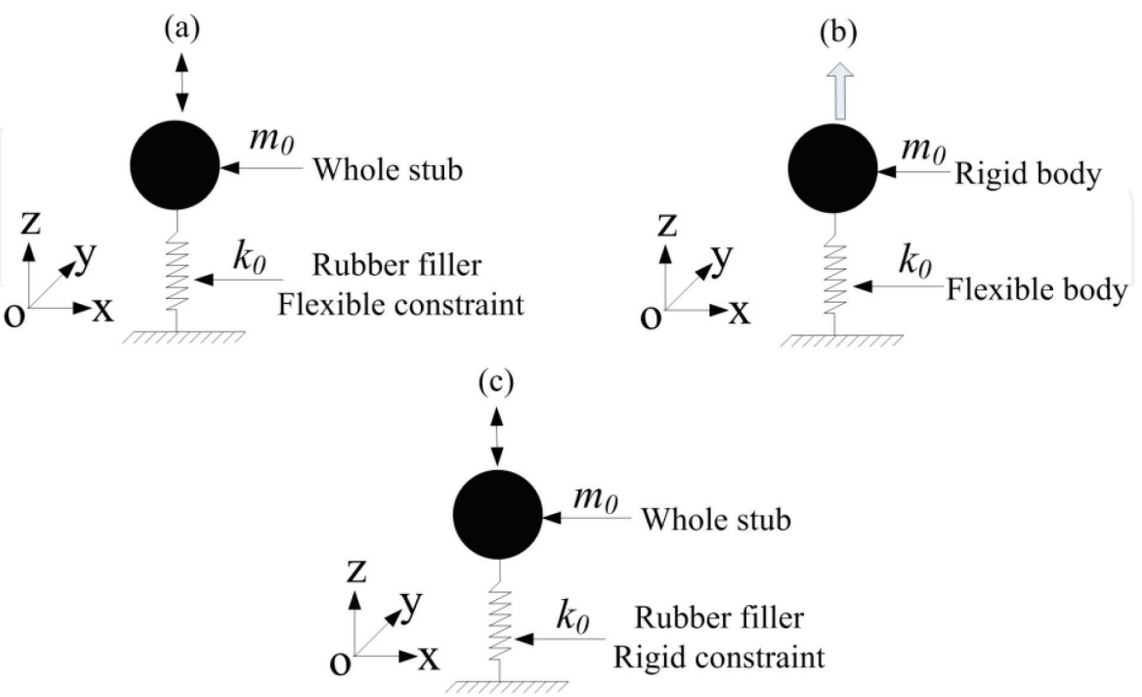

Figure 10.
The equivalent theoretical model of the resonator for formation mechanism of the out-of-plane bandgap of (a) the transition PC plate, (b) the classical PC plate, and (c) the broad complete bandgap metal-matrix embedded phononic crystals.

includes $m_o = 2m_h$ and $m_o = 2m_s + 2m_h$, where m_s denotes the mass of soft stub and m_h denotes the mass of hard stub. It is shown in **Figures 9(c)** and **10(c)** that the frequency is shifted to the lowest frequency range. Compared to the transition PC plate, where the soft stub contacts the rubber filler such that it represents a flexible constraint to the rubber filler (see **Figure 9(a)**), the hard stub contacts the rubber filler in the broad complete bandgap metal-matrix embedded phononic crystals to produce a rigid constraint for the rubber filler (see **Figure 9(c)**). This causes the spring stiffness k_0 ($k_0 = k_{RT}$—the longitudinal stiffness of the rubber filler) to increase, while the lump mass becomes smaller ($2m_s + 2m_h > 2m_h$). This, in turn, not only causes the opening location of the out-of-plane bandgap to shift to higher frequencies but also makes the force F_1 larger than the force F_2. As a result, the out-of-plane bandwidth becomes wider. We conclude that, after introducing the rubber filler, an out-of-plane analogous-rigid mode of the stub was produced, which can reduce the location of the out-of-plane bandgap. Hence, the introduction of a single "hard" stub increases the bandwidth of the out-of-plane bandgap by enhancing the stiffness of the out-of-plane analogous-rigid mode of the stub.

4.2.2 Forming mechanisms of the broad in-plane BGs

Figure 11 displays the magnitudes of the total displacement vectors of a unit cell of the broad complete bandgap metal-matrix embedded phononic crystals, the transition PC plate, and the classical PC plate. The figures correspond to the upper and lower edges of the first in-plane bandgap of each structure. The mode S_2 is a symmetric Lamb mode of the plate. The steel plate vibrates along the xy-plane (in-plane), while the stubs swing in the opposite direction. With respect to the frequencies, the symmetric Lamb mode will be activated, and the in-plane waves can propagate through the phononic-crystal plate in the symmetric Lamb mode. When the frequency of the in-plane waves approaches the first natural frequency of the stub resonator, the resonant mode S_1 will be activated. The stub vibrates in the yz-plane and produces a reacting force to the plate while vibrating in the xy-direction. In that case, the in-plane waves are not able to propagate through the PCs. As a result, an in-plane bandgap opens up. The bandwidth is determined by the coupling between the resonance mode S_1 and the traditional plate mode S_2.

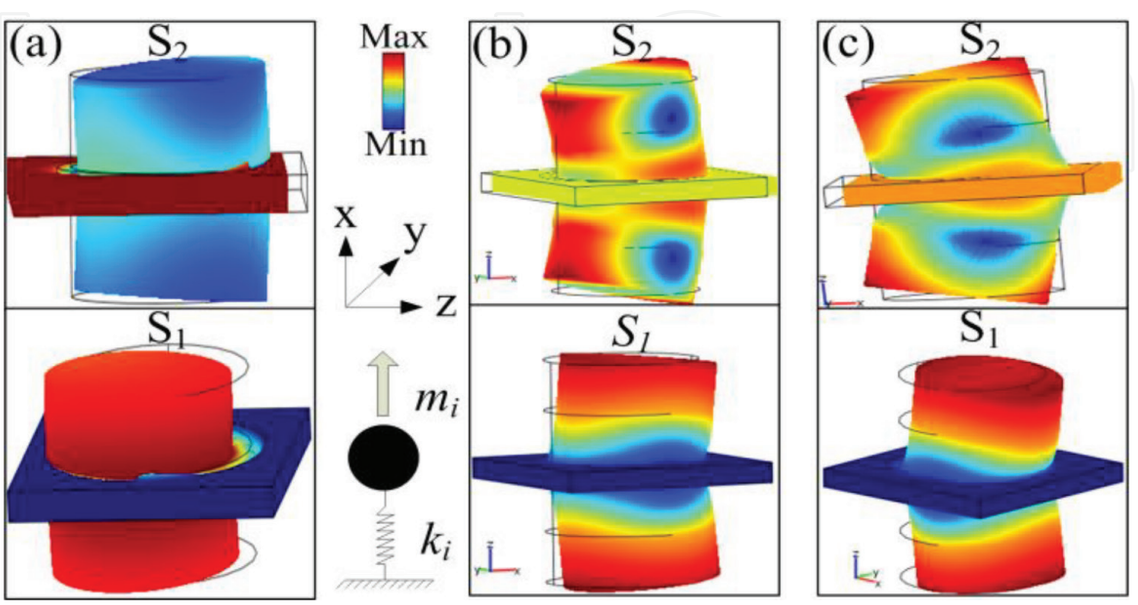

Figure 11.
*The total displacement vector fields for the modes (resonant mode S1, symmetric Lamb mode S2) (a) correspond to **Figure 4(a)**, (b) correspond to **Figure 4(b)**, and (c) correspond to **Figure 4(c)**.*

The coupling strength between the resonance mode S_1 and the traditional plate mode S_2 is determined by the formula

$$F = k_i s_L \tag{10}$$

where s_L is the vibration amplitude of the stub and k_i is the tensional stiffness of the spring.

For both the transition and the classical phononic-crystal plates, the formation mechanism of the in-plane bandgap is shown in **Figure 12(a)** and **(b)**, respectively.

It can be found that the stubs "swing" in the *xy*-plane and produce a reacting force ($F_2 = k_i.s_L = k_{ST}.s_L$, where k_{ST} is the transverse stiffness of the soft stub and s_L is the vibration amplitude of the whole stub) through the soft stub (flexible body) to the plate against the plate vibrating along the *xy*-plane. The soft stub (flexible) acts as a spring ($k_i = k_s$), while the hard stub (rigid body) acts as a mass ($m_i = m_h$), as shown in **Figure 13(a)** and **(b)**, respectively. Hence, both location and bandwidth of the first in-plane bandgap in these structures are the same.

For the broad complete bandgap metal-matrix embedded phononic crystals, it can be found that the displacement fields are distributed across the entire stub (**Figure 11(a)**) to cause an "in-plane analogous-rigid mode" because the whole stub vibrates along the *xy*-plane (in-plane) with a weak constraint, while the frequency is non-zero. It can be observed that the displacement fields of its eigenmodes are distributed throughout the whole stub. This means that the whole stub body moves in the *xy*-plane like a rigid body moves in rigid mode. However, the natural frequency is not 0, and the whole stub is constrained by the rubber filler. Therefore, we refer to the concept of rigid mode and call this type of vibration mode of a whole stub the "in-plane analogous-rigid mode." The formation mechanism of the bandgap is shown in **Figure 12(c)**. The whole stub vibrates in the *xy*-plane and produces a reacting force ($F_1 = k_i.s_L = k_{RL}.s_L$, where k_{RL} is the longitudinal stiffness of the rubber filler and s_L is the vibration amplitude of the whole stub) through the rubber filler to the plate against the plate vibrating in the *xy*-plane.

In this case, the "rubber filler" acts as a spring, where the longitudinal stiffness of the rubber filler acts as the spring, while the whole stub acts as a mass, where

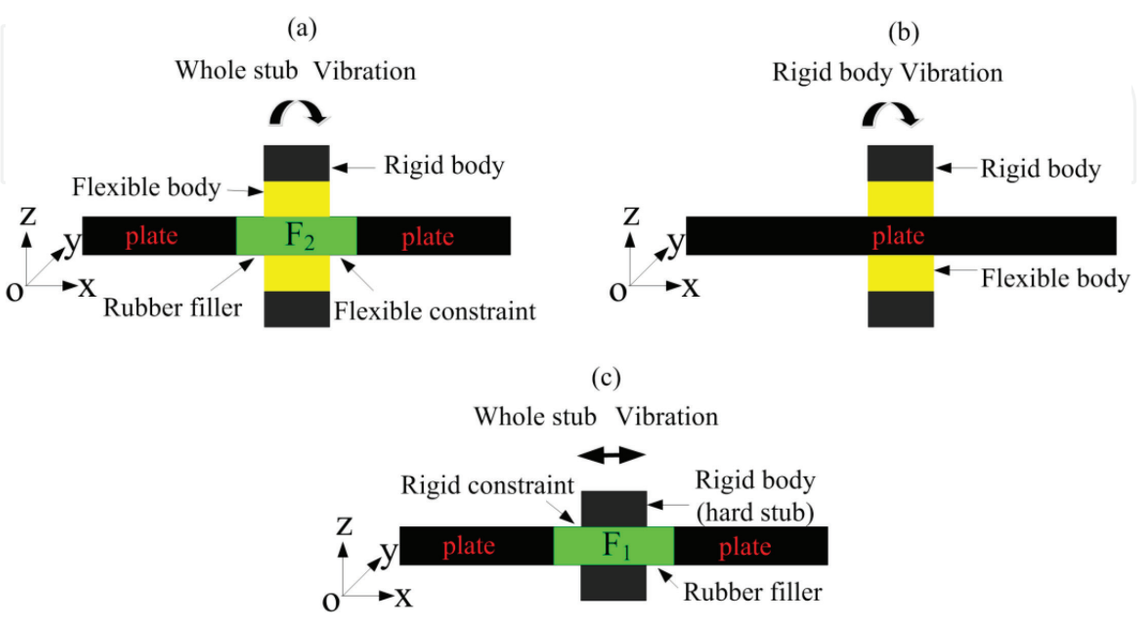

Figure 12.
Formation mechanism process of the bandgap for the in-plane bandgap of (a) the "transition" PC plate, (b) the classical PC plate, and (c) the broad complete bandgap metal-matrix embedded phononic crystals.

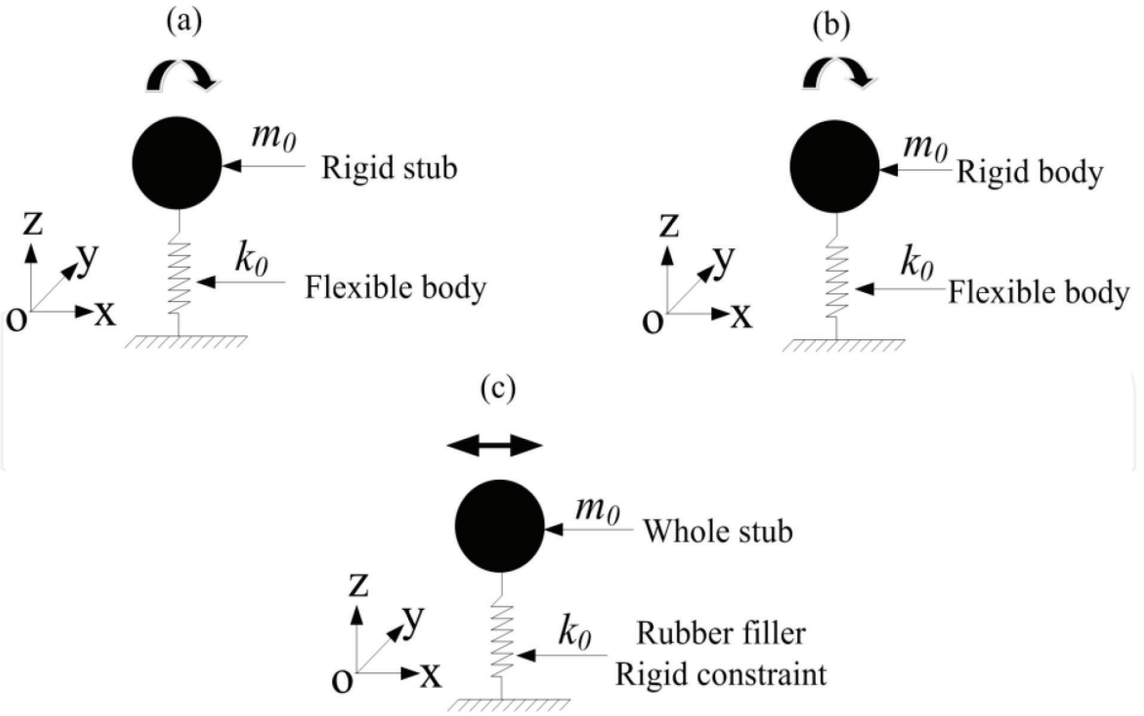

Figure 13.
The equivalent theoretical model of the resonator for formation mechanism of the in-plane bandgap of (a) the "transition" PC plate, (b) the classical PC plate, and (c) the broad complete bandgap metal-matrix embedded phononic crystals.

$m_i = m_h$, and m_h denotes the mass of hard stub (see **Figure 13(c)**). Compared to the transition PC plate, in which the soft stub contacts the rubber filler such that it gives a flexible constraint to the rubber filler, this leads to the soft stub acting as a spring (see **Figure 13(c)**). The hard stub contacts the rubber filler in the broad complete bandgap metal-matrix embedded phononic crystals, which creates a rigid constraint to the rubber filler that causes the rubber filler to act as a spring (see **Figure 13(c)**). This causes the spring stiffness k_i to increase in the broad complete bandgap metal-matrix embedded phononic crystals such that the opening location of the in-plane bandgap is shifted toward higher frequencies. However, it also makes the force F_1 larger than force F_2 and causes the in-plane bandwidth to become broader. We conclude that, after introducing the rubber filler and the single "hard" stub simultaneously, an "in-plane analogous-rigid mode" of the stub is produced, which can increase the bandwidth of the in-plane bandgap.

4.2.3 Forming mechanisms of the broad complete BGs

When the broad out-of-plane bandgaps and broad in-plane bandgaps, which were simultaneously increased by the single "hard" stub, overlap, a wider complete bandgap, in which the out-of-plane and in-plane Lamb waves are prohibited, is created.

It can be concluded that the bandwidth of the bandgap is determined by the resonator mode. After introducing the rubber filler and the single "hard" stub simultaneously, two new resonator modes are produced. One resonator mode is the in-plane analogous-rigid mode, in which the whole stub vibrates along the in-plane plate. The other resonator mode is the out-of-plane analogous-rigid mode, in which the stub vibrates along the out-of-plane plate. They both increase the in-plane and out-of-plane bandgaps, respectively. Two increased bandgaps overlap to produce a broad complete bandgap, in which both the out-of-plane and in-plane Lamb waves are

prohibited. The rubber filler shifts the two kinds of bandgaps simultaneously toward low frequency such that a broad complete bandgap for low frequencies is obtained.

5. The effect of the stubs on the BGs

In order to investigate the effect of the stubs on the complete bandgaps of the metal-matrix embedded phononic crystals [14, 18], we studied the influence of the stub height on the first complete bandgap.

5.1 The effect of the stubs on the lower frequency complete BGs

Figure 14 displays the evolution of the first complete bandgap as a function of the steel-stub height, h_S. We can find that, with the increase of the steel-stub height, both the lower and upper edges of the first complete shift to a lower frequency range firstly and then move to higher frequency range. For example, when the steel-stub height is less than or equal to 3 mm, with the increase of the steel-stub height, the lower edge shifts to lower frequencies, but when the rubber stub height is larger than 3 mm, the lower edge frequency shifts to higher frequencies as the steel-stub height increases.

5.2 The effect of the stubs on the broad complete BGs

In order to investigate the effect of single "hard" stubs on the complete phononic bandgaps of the novel metal-matrix PCs, we studied the effect of the steel-stub height on the first complete bandgap. **Figure 15** displays the evolution of the first complete bandgap as a function of the steel-stub height *h*.

We find that, with the increase of the steel-stub height, the location of the first complete bandgap shifts to a lower frequency range before it shifts to a higher frequency range. Furthermore, the bandwidth of the bandgaps becomes broad. For example, when the steel-stub height is below or equal to 3.5 mm, after increasing the steel-stub height, the location of the bandgaps shifts to lower frequencies. However, when the steel-stub height exceeds 3.5 mm, the location of the bandgaps shifts to higher frequencies as the steel-stub height increases.

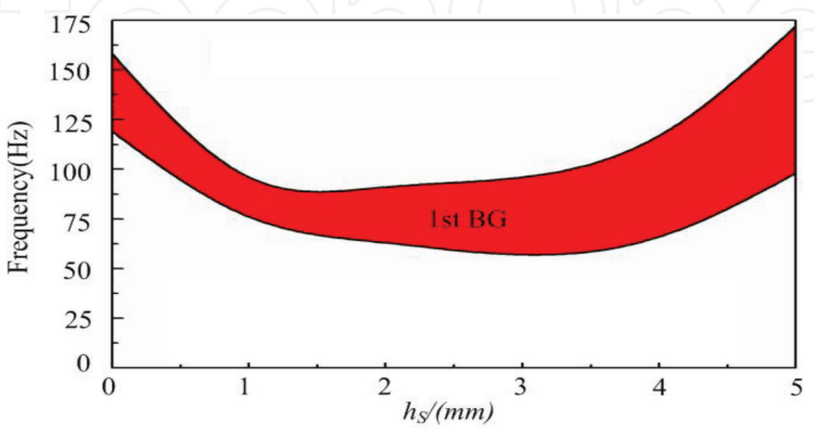

Figure 14.
The evolution of the first complete BG in the lower frequency complete bandgap metal-matrix embedded phononic crystals as a function of the steel-stub height with D = 8 mm, d_{up} = 9 mm, d_{up} = 5 mm, h = 5 mm, e = 1 mm, and a = 10 mm, respectively.

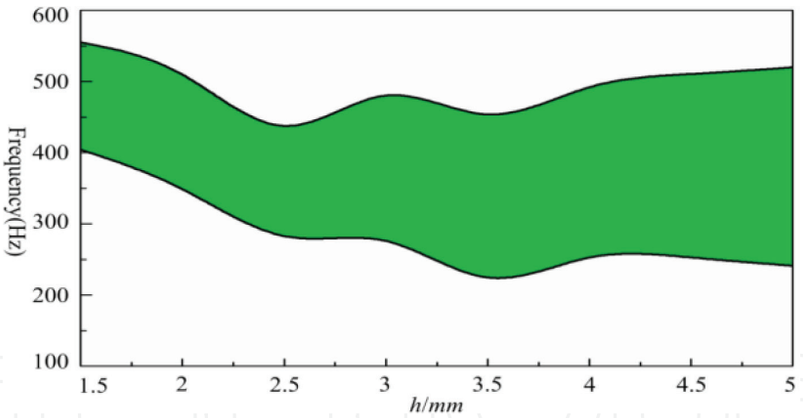

Figure 15.
The evolution of the first bandgap in the proposed phononic-crystal plate with "hard" stubs as a function of steel-stub height with D = 8 mm, d = 7.5 mm, e = 1 mm, and a = 10 mm, respectively.

6. Conclusions

In this chapter, metal-matrix embedded phononic crystals consisting of double-sided stubs (single stubs and composite stubs), which are deposited on a two-dimensional locally resonant phononic crystal plate that consists of an array of rubber fillers embedded in a steel plate, are introduced. The following summaries were drawn [14, 18]:

The spring-mass system of the resonator can be decoupled by introducing the rubber filler, and then the out-of-plane bandgap and the in-plane bandgap can be adjusted into the same lowest frequency range. The out-of-plane bandgap and the in-plane bandgap can be overlapped with each other. As a result, a lower frequency complete bandgap which ranges from 59 to 93 Hz is obtained in the metal-matrix embedded phononic crystals.

Both the out-of-plane and the in-plane phononic bandgap increase after introducing single "hard" cylinder stubs. When introducing the rubber filler and the single "hard" stub simultaneously, two new kinds of resonance modes are produced: an in-plane analogous-rigid modes, where the whole stub vibrates in-plane with the plate, and the other new resonance mode is the out-of-plane analogous-rigid mode, where the whole stub vibrates out-of-plane with respect to the plate. The out-of-plane bandgap increases for the out-of-plane analogous-rigid mode, and the in-plane bandgap increases for the in-plane analogous-rigid mode. Both the out-of-plane and the in-plane analogous-rigid modes are mainly formed due to introducing the single "hard" cylinder stub. The in-plane and out-of-plane bandgaps overlap and produce a broad complete bandgap in the metal-matrix embedded phononic crystals. Within this broad complete bandgap, both the in-plane and out-of-plane Lamb waves are prohibited. The absolute bandwidth of the bandgap for the proposed structure is five times higher than for the classic double-sided stubbed metal-matrix phononic-crystal plate.

The effect of the stub on the bandgaps is investigated. Results show that the location of the bandgaps can be modulated in a significant lower frequency range, and the bandwidth can be expanded in a considerable large frequency range by introducing different composite taper stubs, and the bandwidth can be expanded to a larger frequency range by introducing different "hard" stubs.

The proposed structure provides an effective way for phononic crystals to obtain wide complete bandgaps and lower frequency complete bandgaps (below 100 Hz), which have a potential application in the low-frequency vibration reduction in a practical case.

Acknowledgements

This chapter was supported by the Project of the National Science Foundation of China (No. 51674199).

Author details

Suobin Li[1]*, Yihua Dou[1] and Linkai Niu[2]

1 School of Mechanical Engineering, Xi'an Shiyou University, Xi'an, China

2 College of Mechanical Engineering, Taiyuan University of Technology, Taiyuan, China

*Address all correspondence to: ziyedeyan@stu.xjtu.edu.cn

References

[1] Sigalas M, Economou EN. Band structure of elastic waves in two dimensional systems. Solid State Communications. 1993;**86**(3):141-143

[2] Liu Z, Mao X, et al. Locally resonant sonic materials. Science. 2000;**289**:1734

[3] Meyer R. Vibrational band structure of nanoscale phononic crystals. Physica Status Solidi. 2016;**213**(11):2927-2935

[4] Ho KM, Cheng CK, Yang Z, et al. Broadband locally resonant sonic shields. Applied Physics Letters. 2003;**83**(6):5566-5568

[5] Soliman YM, Su MF, Leseman ZC, et al. Effects of release holes on microscale solid–solid phononic crystals. Applied Physics Letters. 2010;**97**(8):081907

[6] Pennec Y, Djafari-Rouhani B, Larabi H, et al. Low-frequency gaps in a phononic crystal constituted of cylindrical dots deposited on a thin homogeneous plate. Physical Review B. 2008;**78**(10):104105

[7] Wu TT, Huang ZG, Tsai TC, Wu TC. Evidence of complete band gap and resonances in a plate with periodic stubbed surface. Applied Physics Letters. 2008;**93**(11):2022

[8] HSU J. Local resonances-induced low-frequency band gaps in two-dimensional phononic crystals slabs with periodic stepped resonators. Journal of Physics D: Applied Physics. 2011;**44**:055401

[9] Assouar MB, Oudich M. Enlargement of a locally resonant sonic band gap by using double-sided stubbed plate. Applied Physics Letters. 2012;**100**:123506

[10] Zhang SW, Wu JH, Hu ZP. Low-frequency locally resonant band-gaps in phononic crystal plates with periodic spiral resonators. Journal of Applied Physics. 2013;**113**:163511

[11] Song G, Chen J, Han X. Shear horizontal guided wave band gaps in a homogenous plate with periodic tapered surface. Japanese Journal of Applied Physics. 2014;**53**(9):94301

[12] Li Y, Chen T, Wang X, et al. Enlargement of locally resonant sonic band gap by using composite plate-type acousticmetamaterial. Physicals Letters. A. 2015;**379**:412-416

[13] Li S, Chen T, Wang X, et al. Expansion of lower-frequency locally resonant band gaps using a double-sided stubbed composite phononic crystals plate with composite stubs. Physics Letters A. 2016;**380**:2167-2172

[14] Li S, Chen T, Wang X, et al. Lamb waves propagation in a novel metal-matrix phononic crystals plate. Modern Physics Letters B. 2016;**30**:1650338

[15] Li S, Chen T, Xi Y, et al. Forming mechanisms of low-frequency complete band gaps in phononic crystal plate. Journal of Xi'an Jiaotong University. 2016;**50**(12):51-57

[16] Zhoua X, Xub Y, Liua Y, et al. Extending and lowering band gaps by multilayered locally resonant phononic crystals. Applied Acoustics. 2018;**133**:97-106

[17] Zhao H-J, Guo H-W, Gao M-X, et al. Vibration band gaps in double-vibrator pillared phononic crystal plate. Journal of Applied Physics. 2016;**119**:014903

[18] Jiang P. Low-frequency band gap and defect state characteristics in a multi-stub phononic crystal plate with slit structure. Journal of Applied Physics. 2017;**121**:015106

[19] Li Y, Zhu L, Chen T. Plate-type elastic metamaterials for low-frequency broadband elastic wave attenuation. Ultrasonics. 2017;**73**:34-42

[20] Li S, Dou Y, Chen T, et al. A novel metal-matrix phononic-crystal with a low frequency, broad and complete, locally-resonant bandgap. Modern Physics Letters B. 2018;**32**:1850221